HHS Public Access

Author manuscript

Nat Chem. Author manuscript; available in PMC 2021 December 10.

Published in final edited form as:

Nat Chem. 2021 August ; 13(8): 786–791. doi:10.1038/s41557-021-00708-z.

Chiral Lipid Bilayers are Enantioselectively Permeable

Juan Hu[a], **Wesley G. Cochrane**[a], **Alexander X. Jones**[c], **Donna G. Blackmond**[c], **Brian M. Paegel**[a,b]

[a]Department of Pharmaceutical Sciences, 101 Theory, Suite 100, University of California, Irvine, CA 92617

[b]Departments of Chemistry and Biomedical Engineering, 101 Theory, Suite 100, University of California, Irvine, CA 92617

[c]Department of Chemistry, Scripps Research, 10550 N. Torrey Pines Rd., La Jolla, CA 92037

Abstract

Homochiral membrane bilayers organize biological functions in all domains of life. The membrane's permeability–its key property–correlates with a molecule's lipophilicity, but the role of the membrane's rich and uniform stereochemistry as a permeability determinant is largely ignored in empirical and computational measurements. Here, we describe a new approach to measuring permeation using continuously generated microfluidic droplet interface bilayers (DIBs, 480/min) and benchmark this system by monitoring fluorescent dye DIB permeation over time. Permeation of non-fluorescent, alkyne-labeled molecules was measured using a fluorogenic click reaction. DIB transport measurements revealed enantioselective permeation of alkyne-labeled amino acids (Ala, Val, Phe, Pro) and dipeptides through a chiral phospholipid bilayer; the biological L enantiomers permeated faster than D (1.2–6-fold; Ala–Pro). Enantioselective permeation both poses a potentially unanticipated criterion for drug design and offers a kinetic mechanism for the abiotic emergence of homochirality via chiral transfer between sugars, amino acids, and lipids.

Graphical Abstract

Correspondence to Brian M. Paegel (bpaegel@uci.edu).

Author contributions

J.H., W.G.C., and B.M.P. conceived of the research. J.H. performed the experiments. D.G.B. guided the experimental design related to dipeptides. A.X.J. synthesized and characterized dipeptides. J.H. and B.M.P. analyzed the data. All authors wrote the manuscript.

Competing Interests

The authors declare no competing interests.

Supplementary information

Supplementary figures 1–9, methods, and data analysis.

Data and Code Availability

Data supporting the findings of this study are available within this article and its Supplementary Information. Raw data of main figures in the article and R code for general data analysis are available in Figshare with the link https://figshare.com/s/b387496fed3d3befd61d.

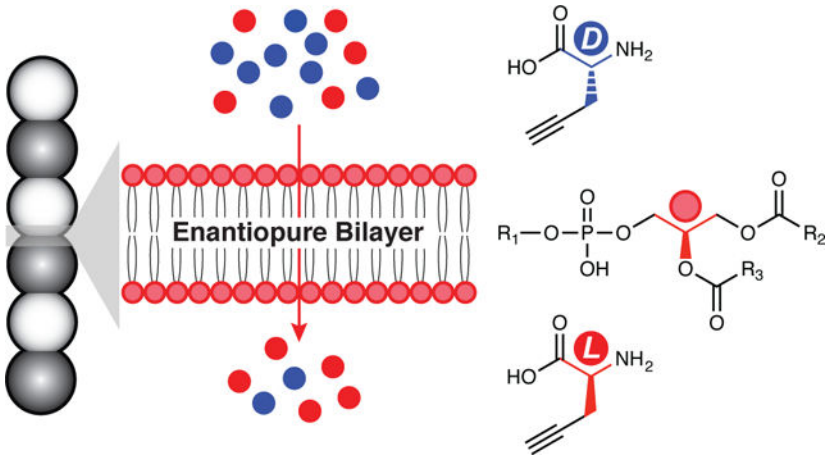

Droplet interface bilayer (DIB) measurements revealed that biological chirality membranes (red glycerol stereocenter) are enantioselectively permeable to biological chirality amino acids (red amino acid). Membrane stereochemistry is necessary and sufficient to drive such enantioselective transport, presenting a new potential route to homochirality.

Introduction

Semi-permeable membrane bilayers, the thermodynamically spontaneous product of amphiphile self assembly,[1,2] are hallmarks of life. Cells universally exploit membranes to associate their genes selfishly with the metabolic activities necessary for survival and to scaffold receptors and channels for interacting with their environment. The ubiquity of membraneous structures in modern biology at once suggests an ancient role for bilayers in the emergence of life[3] and underscores the importance of understanding how membrane biophysical properties influence cellular function and guide drug design.

Permeability is perhaps paramount among the properties of membranes. The Meyer-Overton rule,[4,5] which models membranes as simple diffusion barriers, directly relates a molecule's membrane permeation coefficient to its oil-water partition coefficient. The relationship holds for partition coefficients spanning many orders of magnitude, making it a general tool for predicting permeation. However, molecules with very similar partitioning can exhibit different passive membrane permeation rates.[6–8] Empirical discrepancies from the diffusive barrier model imply that membranes, like all other biomolecules, may participate in complex three-dimensional molecular recognition interactions. The same energetic and steric considerations that define molecular recognition processes therefore should be relevant to molecule-membrane interactions, and consequently permeation. Observation of enantioselective permeation would be the most compelling evidence that membranes are capable of molecular recognition, since enantiomers are physicochemically identical molecules.

Probing the enantioselectivity of interactions between chiral molecules and membrane-bound macromolecules is a textbook feature of drug discovery programs, but such interactions with the plasma membrane remain underappreciated. This is surprising given

that the plasma membrane is a richly chiral environment; virtually every lipid displays its head group on a chiral glycerol, many lipid head groups are chiral themselves, and several lipid acyl chains along with numerous membrane-integral molecules (e.g., sterols, proteins) contain stereocenters. Very few studies have probed the interactions between chiral molecules and chiral membranes, but there is evidence for diastereoselective permeation[6] and enantioselective membrane binding of amino acids[9] and peptides.[10,11] Taken together, these observations suggest that enantioselective permeation likely occurs for all chiral molecules and may be predictable. However, the lack of an appropriately sensitive and general tool for measuring such transport constitutes a major obstacle.

Here, we disclose a microfluidic circuit for making high-sensitivity measurements of membrane transport. The circuit generates trains of phospholipid monolayer-stabilized droplets in contact with each other, thereby forming membrane bilayers at the droplet interfaces.[12,13] These droplet interface bilayers (DIBs) are important in vitro tools that support diverse measurements, from membrane protein insertion to patch clamp electrophysiology.[14–16] Whereas conventional DIB formation is manual and individual, the present approach mediates continuous and automated DIB formation, in turn enabling high-throughput membrane transport measurement. We validate the approach by measuring permeation of fluorescent dye standards, then describe minimal and modular labeling of non-fluorescent molecules with alkynes to monitor their transport via a fluorogenic click reaction.[17] The approach's sensitivity revealed subtle but significant differences in permeation coefficients of enantiomers transporting through a chiral bilayer, illuminating a new consideration in drug design and a new abiotic mechanism for enantioenrichment.

Results and Discussion

Measurement of permeation coefficients ideally entails replicate observations of flux across the subject membrane. We engineered a microfluidic circuit that continuously generates DIBs,[12,14,18] allowing time-resolved observation of molecular transport from a donor droplet to a receiver droplet (Fig.1a). The continuous microfluidic DIB generator integrates droplet formation, synchronization, and incubation (Fig.1b). Donor (AQ1) and receiver (AQ2) droplets in lipid-containing oil streams (OIL1, OIL2) merge at a droplet synchronizer, [19] which separates (OIL3) and pairs donor and receiver droplets. The donor-receiver droplet pairs follow guiding tracks[20] as they exit the synchronizer and enter the serpentine incubation channel (Supplementary Fig.1), which houses the DIB "train," a continuous donor-receiver-donor series of droplets AQ1 and AQ2 droplet generation rates are 4 Hz each (~480 DIBs/min). Laser-induced fluorescence detection at different delay positions in the incubation channel yields time-dependent data for reconstructing permeation curves.

The continuous DIB generator circuit automates and simplifies bilayer formation and permeation measurement. DIB technology significantly expanded the scope of artificial bilayer-based experimentation with facile experimental replication in patch clamp membrane protein studies,[12] and generation of complex multi-compartment membrane-connected networks.[21] DIB formation automation using droplet microfluidics has yielded several promising systems for imaging molecular transport, wherein droplet pairs are precisely positioned and monitored over time.[22–24] These systems have limited throughput, however,

and semi-stochastic droplet-droplet contact further complicates accurate transport measurement. The present device forms hundreds of DIBs per minute in a controlled and continuous process, minimizing variation and greatly enhancing statistical power.

We demonstrated the feasibility of measuring small molecule permeability in DIBs using a series of fluorescent dye standards. Dyes are an ideal testbed because that are directly detectable and have known membrane permeation coefficients, such as the highly membrane-permeable resorufin[25] and rhodamine 110 (R110), and membrane-impermeable carboxylic acids 5(6)- carboxytetramethylrhodamine (cTMR) and 5(6)-carboxyfluorescein (cFAM).[26] Raw droplet fluorescence traces showed membrane-permeable resorufin readily transporting from donor to receiver droplets with increasing incubation time (Supplementary Fig. 2a). Quantitative permeation curves were generated using donor-receiver droplet pair data exclusively (~80% of events), with all non-conforming droplet pattern data removed *post-hoc* (Supplementary Fig. 2b–e). Using these curated data sets, resorufin permeated the DIB fastest followed by R110; cFAM and cTMR were impermeable (Fig.2). Passive permeation is diffusion-limited and, accordingly, permeation data were modeled according to Fick's Law as a single exponential rise to maximum (see Supplementary Information) to obtain membrane permeation coefficients $P_m = 6.5 \pm 0.9 \times 10^{-4}\ cm \cdot s^{-1}$ for resorufin and $1.9 \pm 0.2 \times 10^{-4}\ cm \cdot s^{-1}$ for R110. Measurements of resorufin permeation in DIBs agreed with previously DIB-based measurements $P_m = 1.8 \pm 0.2 \times 10^{-4}\ cm \cdot s^{-1}$.[25] Transport occurred very rapidly in all permeation curves, with donor and receiver reaching equilibrium in < 3 min. Finally, permeation was concentration independent over a broad range of dye concentrations (0.02–50 μM) and decreased upon addition of cholesterol (Supplementary Fig. 3). Reduced membrane permeability of cholesterol-containing DIBs was also consistent with cholesterol's well-known effect on membrane fluidity and permeability.[25,27]

Experimental conditions in the continuous DIB device promote rapid transport equilibration between droplet compartments due to the inherent recirculating flow found in droplets.[28,29] DIB-derived P_m values agree with literature values (Supplementary permeation coefficient calculation).[25] Due to this continuous intradroplet recirculating flow, we also observe the expected concentration-independent permeation without requiring high cargo concentrations to drive transport through the DIB. Quite the opposite, DIB permeation curves readily yield quantifiable P_m even at 20 nM dye.

We next sought a strategy for observing membrane permeation of non-fluorescent small molecules. A fluorogenic click reaction[17] using a membrane-impermeable azide probe (CalFluor 488 Azide, CF-N_3) was adapted to DIBs, wherein donor droplets contain alkyne-labeled small molecule cargo and receiver droplets contain the CF-N_3 probe. Upon permeating the membrane, alkyne cargo reacts with CF-N_3 to yield fluorescent triazole product (Fig. 3a). Four alkynes' membrane permeabilities were monitored (Fig. 3b), with propargylamine (PA) permeating most rapidly followed by unnatural amino acids L-propargylglycine (L-Pra), D-propargylglycine (D-Pra), and N-propargylglycinamide (Gly-yne). N-propargylamides of proline, phenylalanine, valine, and alanine were also prepared. For all amino acid enantiomers tested, the L enantiomer permeated more rapidly than D (6- , 4- , 2-, and 1.2-fold, respectively; Fig. 3c). Fluorogenic click reaction progress for all

enantiomer pairs (L-Pra and D-Pra; L-Pro/Phe/Val/Ala-yne and D-Pro/Phe/Val/Ala-yne) was statistically identical (Supplementary Fig. 4).

The fluorogenic click reaction permitted the detection of minimally labeled small molecule transport, revealing differential permeation of enantiomer pairs. As a canonical click reactant,[30] the alkyne adds minimal mass (25 Da) with orthogonal reactivity, making it straightforward for labeling molecules with diverse functional groups. Alkynes also minimally affect cLogP (and thus permeability) when compared with fluorescent dye labeling and no labeling (Supplementary Fig. 8).[31] The alkyne test panel exemplifies the diverse functionality available for labeling other molecules (Pra, PA) and further included multiple examples of alkyne-labeled molecules (Gly-yne, Ala-yne, Val-yne, Phe-yne, Pro-yne). L-Pra and D-Pra differentially permeated the DIB; L-Pra permeated 2.4-fold more rapidly than D-Pra. Control experiments confirmed that this differential permeability was not due to reactivity differences with CF-N_3. Similar analysis of L- and D-Pro/Phe/Val/Ala-yne also showed permeation favoring the L enantiomer. Enantioselective permeation correlated with functional group steric bulk at the stereocenter. Proline exhibited outsized enantioselective permeation, possibly pointing to an important role for conformational constraint. These results collectively suggest that the DOPC/POPC bilayers with biological head group chirality are enantioselectively permeable to amino acid derivatives with biological chirality.

Single stereocenter-induced enantioselective permeation in simple amino acids prompted an investigation of dipeptide stereoselective permeation. The four diastereomers of a primitive enantioselectively catalytic Pro-Val dipeptide[32,33] —Pro-Val—L-Pro-L-Val (PV), L-Pro-D-Val (Pv), D-Pro-D-Val (pv), and D-Pro-L-Val (pV)—were alkyne-labeled as N-propargylamides and were equally reactive toward CF-N_3 (Supplementary Fig. 4). Subsequent DIB transport studies measuring permeation coefficients based on observation of the fluorogenic click reaction progress, $P_{m,obs}$, revealed that PV ($P_{m,obs}$ = 3.0 ± 1.0 × 10^{-4} $cm \cdot s^{-1}$) permeated fastest with P_m ~8-fold and ~10-fold greater than Pv ($P_{m,obs}$ = 4.0 ± 0.4 × 10^{-5} $cm \cdot s^{-1}$) and pv ($P_{m,obs}$ = 3.0 ± 0.5 × 10^{-5} $cm \cdot s^{-1}$) , respectively, but only ~2-fold higher than pV (1.3 ± 0.3 × 10^{-4} $cm \cdot s^{-1}$) (Fig. 4). To confirm the role of membrane chirality, we diluted chiral phospholipid DIB content to 1 mol% in achiral oleic acid. Transport became independent of dipeptide chirality and membrane permeability was increased overall (Supplementary Fig. 6c). We also reversed the lipid stereochemical configuration from *R*- (biological) to *S*- (abiological). DIBs composed of *S* phospholipids exhibited opposite enantioselective permeability for the proline and proline-valine dipeptide (Fig. 4b and supplementary Fig. 6d–h).

Analysis of dipeptide permeation revealed more complex relationships between stereochemical configuration and biological membrane permeability. Enantioselective DOPC/POPC membrane permeability favoring PV over pv agreed with analogous assays of amino acid permeation: the biological stereochemistry drove selective permeation over the abiological stereochemistry. One would anticipate that diastereomers Pv and pV exhibit intermediate permeation rate. While the rate for pV was intermediate, Pv permeation was indistinguishable from pv. The C-terminal residue stereochemistry seems to be the determinant of enantioselective permeation. Proximity of nonpolar groups (isopropyl,

alkyne) to this stereocenter may drive this trend, but confirming this interpretation will require additional structure-activity data. Controls again confirmed no significant difference in intrinsic CF-N_3 probe reactivity between the various dipeptide N-propargylamides, thus stereoselective transport was not a kinetic artifact of the fluorogenic click reaction (Supplementary Fig. 4). Furthermore, permeation experiments using either achiral oleic acid or enantiomers of biological phospholipids DIBs[34] proved that enantioselective permeation resulted from interactions between the chiral permeant and the chiral phospholipid headgroup. Headgroup chirality is necessary and sufficient to drive enantioselective permeation. Although we cannot rule out the presence of oil in the bilayer[35], squalene is achiral and present in all experiments, allowing us to rule it out as a determinant of enantioselective permeation.

These studies establish enantioselective permeability as a property of chiral membrane bilayers. This phenomenon is expected based on much more well-known accounts of chiral molecular recognition (e.g., proteins and small molecules), although there are scant studies of membrane chirality playing such a role. Phenylproline tetrapeptide blood-brain barrier “shuttles” exhibited diastereoselective permeability in PAMPA assays and some enantiomer pairs permeated quite differently.[36] Physical interactions also occur between membranes and permeants, such as binding interactions between chiral bilayers and bioactive macrocyclic peptides,[10] peptide amphiphile supramolecular assemblies,[9] or L-amino acids.[11] Our observations that L amino acids and dipeptides enantioselectively permeate chiral bilayers with biological stereochemistry align with these findings, suggesting that lipid head group binding affinities may be a primary determinant of enantioselective permeation.

The dense and uniform stereochemistry of the bilayer surface and cellular homochirality are the products of contemporary biological metabolism, but these studies may also illuminate a role for membrane permeability in the emergence of homochirality at life’s origins. A key question concerns mechanisms for enantioenriching pools of building blocks, such as sugars or amino acids, from racemates or achiral starting materials.[37] Candidate processes include attrition-enhanced deracemization,[38–40] enantioselective autocatalysis,[41–43] and kinetic resolution.[44] Enantioselective permeation may be another mechanism for kinetic resolution whereby the membrane bilayer is a filter that enriches the intracellular space with the chirality that is metabolically complementary to the membrane’s intrinsic enantioselective permeability. Enantioenrichment would then occur in the limit of protocells spontaneously growing and dividing[45] more rapidly than equilibration.

Membrane permeation could also provide an early mechanism for selection.[6] Our results demonstrate the stereoselective permeation of prebiotically plausible dipeptide catalysts.[46] Dipeptides catalyze important bond-forming reactions,[32,33,46] supply membrane-forming amphiphiles to promote protocellular growth and division,[47] and, most importantly, form spontaneously in several prebiotically plausible reactions that yield highly complex, racemic mixtures.[48–50] Permeation could provide a mechanism for the enantioselection of catalysts from these mixtures, indirectly imprinting the intracellular milieu with the bilayer’s chirality and subsequently driving direct transfer of amino acid chirality to sugars and other classes of molecules via asymmetric synthesis.[32,46]

If one considers enantioselective membrane permeation a prebiotically plausible route to homochirality, then a route to enantioenriched bilayer membranes is necessary. To form such bilayers would require a feedstock of enantioenriched chiral amphiphiles. Amphiphiles could be deracemized by one of the processes discussed above, or by a sergeants-and-soldiers process wherein amphiphile supramolecular assembly may lend itself to chiral amplification.[1,51,52] Chirality-dependent emergent properties of amphiphile assemblies, including vesicular transition temperature[53] and bilayer gelation energetics,[54,55] offer alternative routes to amphiphile enantioenrichment. Subsequent assembly of enantioenriched amphiphiles into protocells would provide the selectively permeable compartments for molecular evolution[45,56] that could also participate in systems-level prebiotic processes. Enantioselective permeation may be similarly coupled with various asymmetric physical and chemical processes to enhance enantioenrichment.[57,58] A systematic study of prebiotically plausible chiral amphiphile bilayer enantioselective permeabilities would illuminate ideal vesicle composition for prebiotic enantioenrichment studies.

Conclusions

These studies lay the groundwork for making scalable, high-throughput membrane permeability measurements. Our approach couples automated DIB formation with a general method for sensing the permeation of fluorescent molecules directly and sensing non-fluorescent molecules using a minimal alkyne label. The method is exquisitely sensitive in that it readily reveals differential permeation of single-stereocenter enantiomers and the more complex patterns of dipeptide stereoselective permeation. The molecular properties underpinning permeation may be more broadly assessed using alkyne-labeled combinatorial chemical libraries in flow with DIB trains and photochemical cleavage.[59,60] These studies will provide large-scale empirical structure-activity data that will shed light on these more nuanced determinants of membrane permeation, addressing broad-ranging applications in pharmacokinetic property tuning to fundamental studies of symmetry breaking at the origins of life.

Supplementary Material

Refer to Web version on PubMed Central for supplementary material.

Acknowledgements

Funding from the Simons Foundation through the Simons Collaboration on the Origins of Life (SCOL 287625), the National Institutes of Health (R01GM120491), and the National Science Foundation (1255250) is gratefully acknowledged.

References

1. Luisi PL, Walde P & Oberholzer T Lipid vesicles as possible intermediates in the origin of life. Curr. Opin. Colloid Interface Sci 4, 33–39 (1999).
2. Deamer DW & Dworkin JP Chemistry and physics of primitive membranes. Top. Curr. Chem 259, 1–27 (2005).
3. Joyce GF & Szostak JW Protocells and RNA Self-Replication. Cold Spring Harb. Perspect. Biol 10, a034801 (2018). [PubMed: 30181195]
4. Overton E Vierteljahrsschr. Naturforsch. Ges. Zurich 44, 88–135 (1899).

5. Al-Awqati Q One hundred years of membrane permeability: Does overton still rule? Nat. Cell Biol 1, E201–E202 (1999). [PubMed: 10587658]
6. Sacerdote MG & Szostak JW Semipermeable lipid bilayers exhibit diastereoselectivity favoring ribose. Proc. Natl. Acad. Sci. U. S. A 102, 6004–8 (2005). [PubMed: 15831588]
7. Smith DJ, Leal LG, Mitragotri S & Shell MS Nanoparticle transport across model cellular membranes: When do solubility-diffusion models break down? J. Phys. D. Appl. Phys 51, 4004 (2018).
8. Corti G, Maestrelli F, Cirri M, Zerrouk N & Mura P Development and evaluation of an in vitro method for prediction of human drug absorption: II. Demonstration of the method suitability. Eur. J. Pharm. Sci 27, 354–362 (2006). [PubMed: 16364612]
9. Sato K, Ji W, Álvarez Z, Palmer LC & Stupp SI Chiral recognition of lipid bilayer membranes by supramolecular assemblies of peptide amphiphiles. ACS Biomater. Sci. Eng 5, 2786–2792 (2019). [PubMed: 33405611]
10. Henriques ST, Peacock H, Benfield AH, Wang CK & Craik DJ Is the mirror image a true reflection? Intrinsic membrane chirality modulates peptide binding. J. Am. Chem. Soc 141, 20460–20469 (2019). [PubMed: 31765148]
11. Ishigami T, Suga K & Umakoshi H Chiral recognition of L -amino acids on liposomes prepared with L -phospholipid. ACS Appl. Mater. Interfaces 7, 21065–21072 (2015). [PubMed: 26339952]
12. Funakoshi K, Suzuki H & Takeuchi S Lipid bilayer formation by contacting monolayers in a microfluidic device for membrane protein analysis. Anal. Chem 78, 8169–8174 (2006). [PubMed: 17165804]
13. Venkatesan GA et al. Adsorption kinetics dictate monolayer self-assembly for both lipid-in and lipid-out approaches to droplet interface bilayer formation. Langmuir 31, 12883–12893 (2015). [PubMed: 26556227]
14. Holden MA, Needham D & Bayley H Functional bionetworks from nanoliter water droplets. J. Am. Chem. Soc 129, 8650–8655 (2007). [PubMed: 17571891]
15. Bayley H et al. Droplet interface bilayers. Mol. Biosyst 4, 1191–1208 (2008). [PubMed: 19396383]
16. Maglia G et al. Droplet networks with incorporated protein diodes show collective properties. Nat. Nanotechnol 4, 437–440 (2009). [PubMed: 19581896]
17. Shieh P et al. CalFluors: a universal motif for fluorogenic azide probes across the visible spectrum. J. Am. Chem. Soc 137, 7145–7151 (2015). [PubMed: 25902190]
18. Tsofina LM, Liberman EA & Babakov AV Production of bimolecular protein-lipid membranes in aqueous solution. Nature 212, 681–683 (1966).
19. Xu L, Lee H, Panchapakesan R & Oh KW Fusion and sorting of two parallel trains of droplets using a railroad-like channel network and guiding tracks. Lab Chip 12, 3936 (2012). [PubMed: 22814673]
20. Abbyad P, Dangla R, Alexandrou A & Baroud CN Rails and anchors: Guiding and trapping droplet microreactors in two dimensions. Lab Chip 11, 813–821 (2011). [PubMed: 21060946]
21. Holden MA, Needham D & Bayley H Functional bionetworks from nanoliter water droplets. J. Am. Chem. Soc 129, 8650–8655 (2007). [PubMed: 17571891]
22. Czekalska MA, Kaminski TS, Makuch K & Garstecki P Passive and parallel microfluidic formation of droplet interface bilayers (DIBs) for measurement of leakage of small molecules through artificial phospholipid membranes. Sensors Actuators, B Chem 286, 258–265 (2019).
23. Carreras P et al. A microfluidic platform for size-dependent generation of droplet interface bilayer networks on rails. Biomicrofluidics 9, 1–7 (2015).
24. Bai Y et al. A double droplet trap system for studying mass transport across a droplet-droplet interface. Lab Chip 10, 1281–1285 (2010). [PubMed: 20445881]
25. Barlow NE et al. Rheological droplet interface bilayers (rheo-DIBs): Probing the unstirred water layer effect on membrane permeability via spinning disk induced shear stress. Sci. Rep 7, 1–12 (2017). [PubMed: 28127051]
26. Fischer H, Kansy M, Avdeef A & Senner F Permeation of permanently positive charged molecules through artificial membranes—influence of physico-chemical properties. Eur. J. Pharm. Sci 31, 32–42 (2007). [PubMed: 17416489]

27. Huang J & Feigenson GW A microscopic interaction model of maximum solubility of cholesterol in lipid bilayers. Biophys. J 76, 2142–2157 (1999). [PubMed: 10096908]
28. Song H & Ismagilov RF Millisecond kinetics on a microfluidic chip using nanoliters of reagents. J. Am. Chem. Soc 125, 14613–14619 (2003). [PubMed: 14624612]
29. Stone ZB & Stone HA Imaging and quantifying mixing in a model droplet micromixer. Phys. Fluids 17, 1–11 (2005).
30. Kolb HC, Finn MG & Sharpless KB Click chemistry: diverse chemical function from a few good reactions. Angew. Chemie Int. Ed 40, 2004–2021 (2001).
31. Morimoto J, Amano R, Ono T & Sando S A parallel permeability assay of peptides across artificial membranes and cell monolayers using a fluorogenic reaction. Org. Biomol. Chem 17, 2887–2891 (2019). [PubMed: 30810151]
32. Chen YH, Sung PH & Sung K Synthesis of proline-derived dipeptides and their catalytic enantioselective direct aldol reactions: Catalyst, solvent, additive and temperature effects. Amino Acids 38, 839–845 (2010). [PubMed: 19370392]
33. Tang Z et al. Small peptides catalyze highly enantioselective direct aldol reactions of aldehydes with hydroxyacetone: Unprecedented regiocontrol in aqueous media. Org. Lett 6, 2285–2287 (2004). [PubMed: 15200341]
34. Budin I & Szostak JW Physical effects underlying the transition from primitive to modern cell membranes. Proc. Natl. Acad. Sci. U. S. A 108, 5249–5254 (2011). [PubMed: 21402937]
35. Hauß T, Dante S, Dencher NA & Haines TH Squalane is in the midplane of the lipid bilayer: Implications for its function as a proton permeability barrier. Biochim. Biophys. Acta - Bioenerg 1556, 149–154 (2002).
36. Arranz-Gibert P et al. Lipid bilayer crossing-the gate of symmetry. Water-soluble phenylproline-based blood-brain barrier shuttles. J. Am. Chem. Soc 137, 7357–7364 (2015). [PubMed: 25992679]
37. Blackmond DG The origin of biological homochirality. Cold Spring Harb. Perspect. Biol 11, a032540 (2019). [PubMed: 30824575]
38. Viedma C Chiral symmetry breaking during crystallization: Complete chiral purity induced by nonlinear autocatalysis and recycling. Phys. Rev. Lett 94, 065504 (2005). [PubMed: 15783745]
39. Noorduin WL et al. Emergence of a single solid chiral state from a nearly racemic amino acid derivative. J. Am. Chem. Soc 130, 1158–1159 (2008). [PubMed: 18173274]
40. Viedma C, Ortiz JE, De Torres T, Izumi T & Blackmond DG Evolution of solid phase homochirality for a proteinogenic amino acid. J. Am. Chem. Soc 130, 15274–15275 (2008). [PubMed: 18954052]
41. Soai K, Shibata T, Morioka H, K. C. Excess of a Chiral Molecule. Nature 378, 767–768 (1995).
42. Blackmond DG, McMillan CR, Ramdeehul S, Schorm A & Brown JM Origins of asymmetric amplification in autocatalytic alkylzinc additions [3]. J. Am. Chem. Soc 123, 10103–10104 (2001). [PubMed: 11592892]
43. Blackmond DG Autocatalytic Models for the Origin of Biological Homochirality. Chem. Rev 120, 4831–4847 (2019). [PubMed: 31797671]
44. Wagner AJ, Zubarev DY, Aspuru-Guzik A & Blackmond DG Chiral sugars drive enantioenrichment in prebiotic amino acid synthesis. ACS Cent. Sci 3, 322–328 (2017). [PubMed: 28470050]
45. Zhu TF & Szostak JW Coupled growth and division of model protocell membranes. J. Am. Chem. Soc 131, 5705–5713 (2009). [PubMed: 19323552]
46. Weber AL & Pizzarello S The peptide-catalyzed stereospecific synthesis of tetroses: A possible model for prebiotic molecular evolution. Proc. Natl. Acad. Sci. U. S. A 103, 12713–12717 (2006). [PubMed: 16905650]
47. Adamala K & Szostak JW Competition between model protocells driven by an encapsulated catalyst. Nat. Chem 5, 495–501 (2013). [PubMed: 23695631]
48. Gillams R & Jia T Mineral surface-templated self-assembling systems: Case studies from nanoscience and surface science towards origins of life research. Life 8, 10 (2018).

49. Danger G, Charlot S, Boiteau L & Pascal R Activation of carboxyl group with cyanate: Peptide bond formation from dicarboxylic acids. Amino Acids 42, 2331–2341 (2012). [PubMed: 21769498]
50. Leman L, Orgel L & Ghadiri MR Carbonyl sulfide-mediated prebiotic formation of peptides. Science 306, 283–286 (2004). [PubMed: 15472077]
51. Green MM et al. Macromolecular stereochemistry: the out-of-proportion influence of optically active comonomers on the conformational characteristics of polyisocyanates. the sergeants and soldiers experiment. J. Am. Chem. Soc 111, 6452–6454 (1989).
52. Palmans ARA & Meijer EW Amplification of chirality in dynamic supramolecular aggregates. Angew. Chemie Int. Ed 46, 8948–8968 (2007).
53. Morigaki K, Dallavalle S, Walde P, Colonna S & Luisi PL Autopoietic self-reproduction of chiral fatty acid vesicles. J. Am. Chem. Soc 119, 292–301 (1997).
54. Grahame DAS et al. Influence of chirality on the modes of self-assembly of 12-hydroxystearic acid in molecular gels of mineral oil. Soft Matter 7, 7359–7365 (2011).
55. Peng J et al. New dicholesteryl-based gelators: Chirality and spacer length effect. Langmuir 24, 2992–3000 (2008). [PubMed: 18294019]
56. Chen IA, Roberts RW & Szostak JW The emergence of competition between model protocells. Science 305, 1474–1476 (2004). [PubMed: 15353806]
57. Breslow R & Cheng ZL L-amino acids catalyze the formation of an excess of D-glyceraldehyde, and thus of other D sugars, under credible prebiotic conditions. Proc. Natl. Acad. Sci. U. S. A 107, 5723–5725 (2010). [PubMed: 20231487]
58. Hein JE, Tse E & Blackmond DG A route to enantiopure RNA precursors from nearly racemic starting materials. Nat. Chem 3, 704–706 (2011). [PubMed: 21860459]
59. Price AK, MacConnell AB & Paegel BM hνSABR: photochemical dose-response bead screening in droplets. Anal. Chem 88, 2904–2911 (2016). [PubMed: 26815064]
60. Cochrane WG et al. Activity-based DNA-encoded library screening. ACS Comb. Sci 21, 425–435 (2019). [PubMed: 30884226]

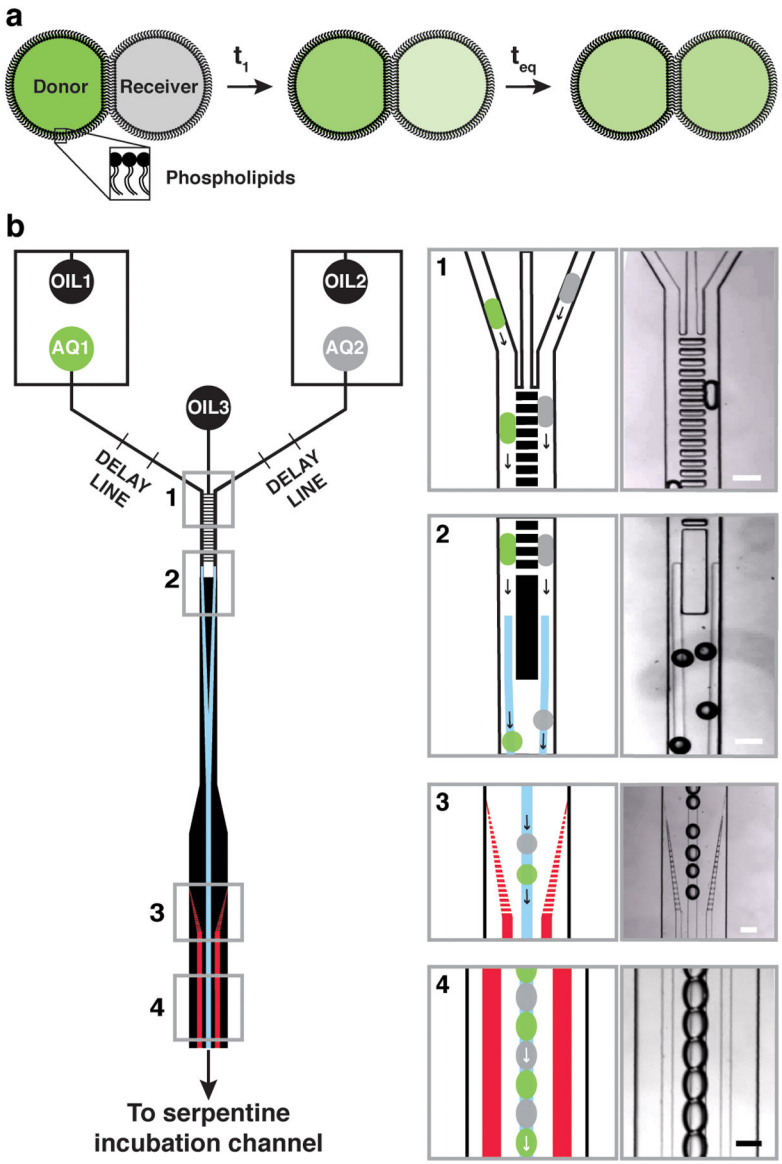

Figure 1. Droplet interface bilayer (DIB) permeation assay and circuit schematic.

(**a**) As time progresses, donor and receiver droplet cargo concentrations equilibrate via passive diffusion of cargo (green) through the DIB from donor to receiver. (**b**) The microfluidic circuit contains two droplet generators with separate aqueous (AQ1, AQ2) and oil inlets (OIL1, OIL2). The droplet generators produce two populations: donor droplets (AQ1) and receiver droplets (AQ2). Donor droplets contain the test compound (green) and the receiver droplets contain buffer (gray). Droplets flow through a delay line, which provides sufficient time for a water-oil interface-stabilizing phospholipid monolayer to form. A third oil inlet (OIL3) further separates droplets entering the droplet synchronizer (1), which orders droplets in alternating donor-receiver-donor fashion. A transition channel with guiding tracks (2) directs the ordered droplets into the incubation channel sequentially. The transition channel (3) merges the donor and receiver droplet flows and widens to facilitate droplet-droplet contact with concomitant DIB formation. The incubation channel (4) houses

the DIB train, an alternating and connected series of donor and receiver droplets. Donor-to-receiver transport occurs as the DIB train traverses the serpentine incubation channel (Supplementary Fig. 1). Micrographs (right) depict device operation. Scale = 100 μm

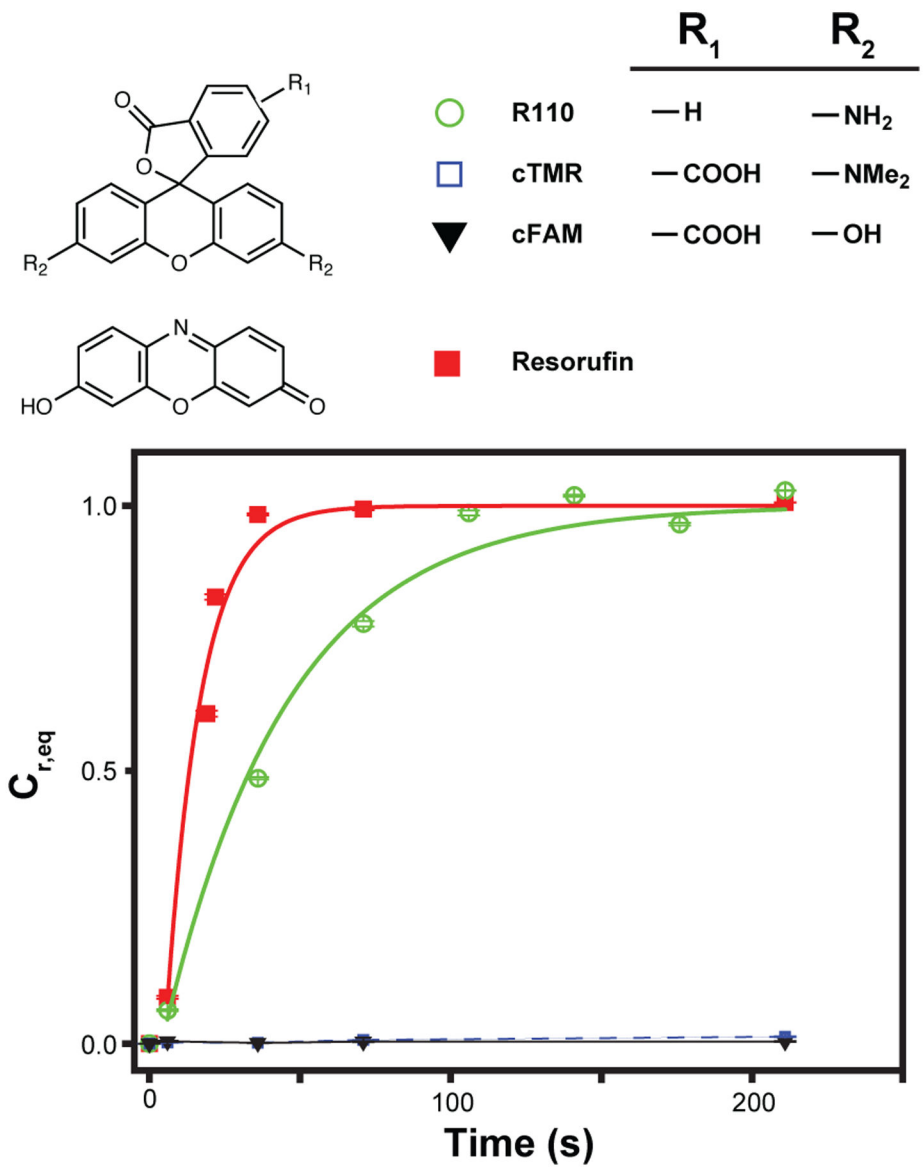

Figure 2. Fluorescent dye cargo permeation measurements.

Permeation was measured for resorufin (red squares), R110 (green circles), cTMR (magenta squares), and cFAM (inverted black triangles) dye cargoes. Permeation coefficients, P_m, were determined by fitting an exponential model, $y = 1 - A \cdot e^{-kt}$, to the equilibrium-normalized receiver droplet transient cargo concentration, $C_{r,eq}$, where C_r is the mean receiver cargo concentration. Error bars indicate the standard deviation of the mean.

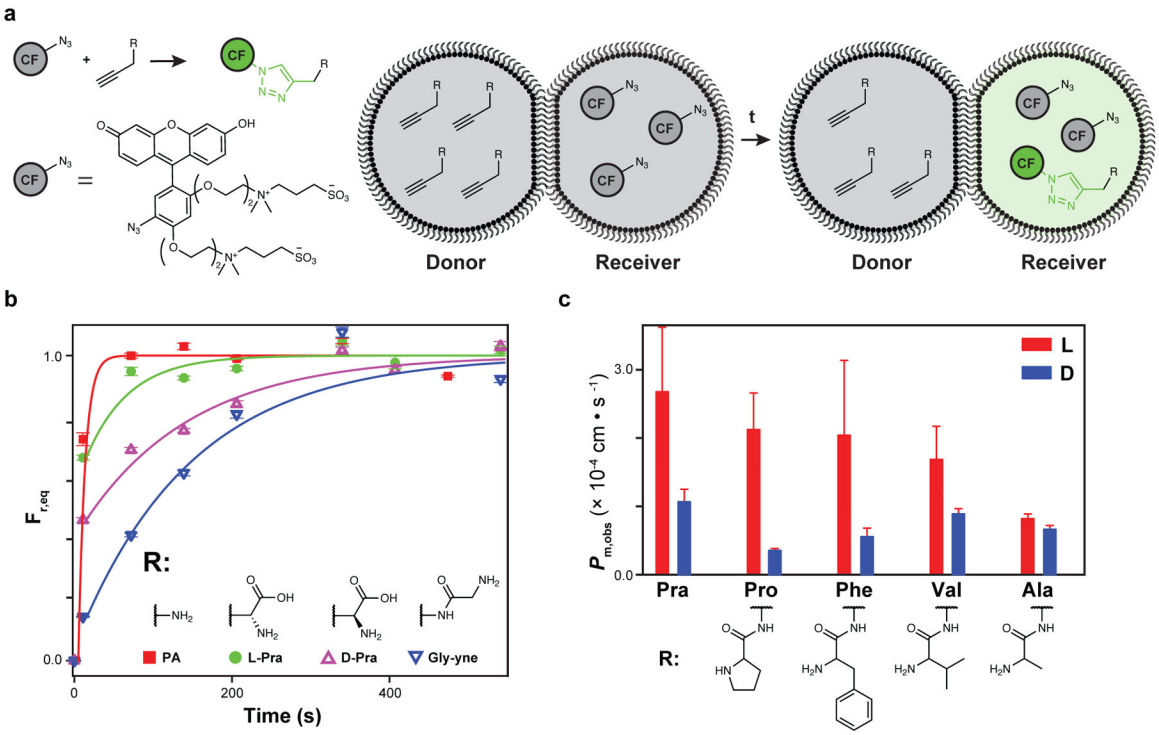

Figure 3. Permeation measurement of alkyne-labeled compounds.

(**a**) CalFluor 488 azide probe (CF-N_3, gray) reacts with alkyne-labeled compounds to yield fluorescent triazole product (green). Alkyne-labeled donor droplet cargo permeates the DIB, entering the receiver droplet containing membrane-impermeable CF-N_3. Evolution of fluorescence from triazole click reaction product formation transduces cargo permeation. (**b**) Propargylamine (PA, red squares), L-propargylglycine (L-Pra, green circles), D-propargylglycine (D-Pra, magenta triangles), and N-propargylglycinamide (Gly-yne, inverted blue triangles) permeation was observed in the DIB chip using CF-N_3. Receiver droplet fluorescence was normalized to donor droplet fluorescence, giving the droplet fluorescence ratio, F_r. Instantaneous F_r values were normalized to F_r at equilibrium, giving $F_{r,eq}$. DOPC/POPC/CH lipidic oil was applied for DIB formation. Error bars reflect standard deviation of the mean. (**c**) Transport data (Supplementary Fig. 5 and 6b) were fit to the exponential model to obtain the membrane permeation coefficient, $P_{m,obs}$ for N-propargylamides of D- and L-propargylglycine / proline / phenylalanine / valine / alanine (L-/D-Pra, L-/D-Pro-yne, L-/D-Phe-yne, L-/D-Val-yne and L-/D-Ala-yne). DOPC/POPC lipidic oil was applied for DIB formation. Error bars reflect regression standard error.

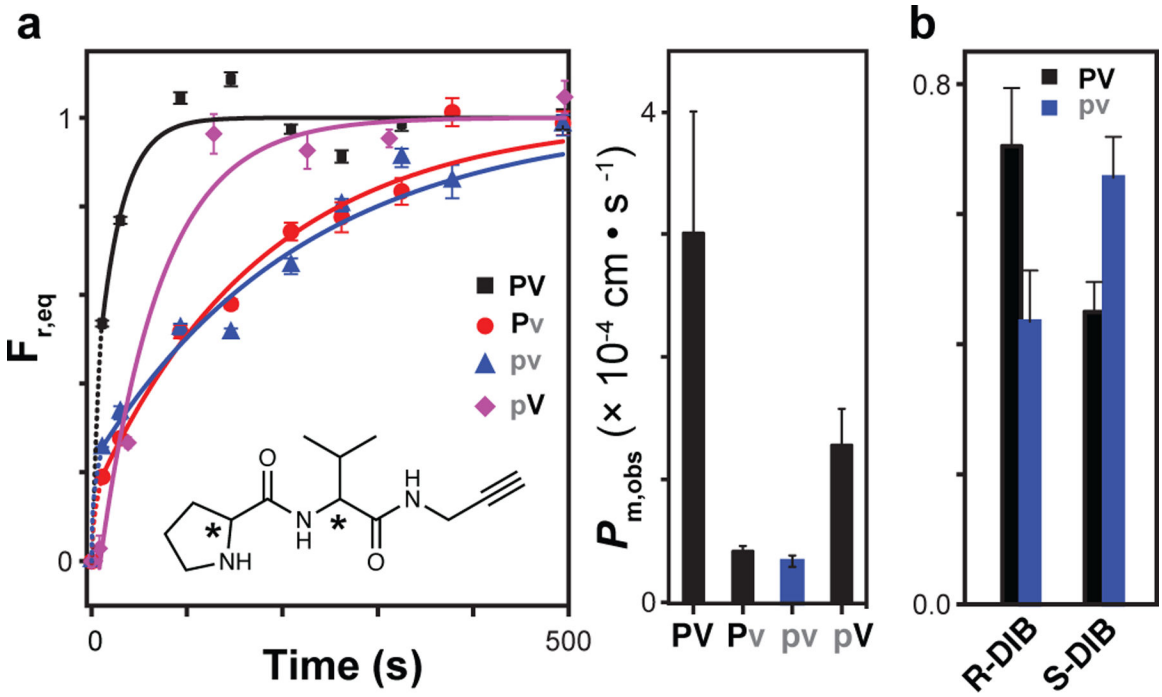

Figure 4. Permeability measurement of alkyne-labeled dipeptide diastereomers.

(a) N-propargylamides of proline-valine dipeptides L-proline-L-valine (PV), L-proline-D-valine (Pv), D-proline-D-valine (pv) and D-proline-L-valine (pV) exhibited stereoselective permeability; phospholipid bilayers (DOPC/POPC) are most permeable to PV. Error bars reflect standard deviation of the mean. Asterisks indicate stereocenters; data were fit to the exponential model as previously described to obtain the membrane permeation coefficient, $P_{m,obs}$. Error bars reflect regression standard error. (b) Enantioselective permeability of *R*-DIB membranes (biological chirality) toward L stereochemistry reversed for *S*-DIB membranes (abiological chirality), which were enantioselectively permeable toward D stereochemistry. Error bars reflect regression standard error. (Transport data in supplementary Fig. 6d–e.)